Confocal Raman microscopy can quantify advanced glycation end product (AGE) modifications in Bruch's membrane leading to accurate, nondestructive prediction of ocular aging

Josephine V. Glenn,*[,1] J. Renwick Beattie,[†,‡,1] Lindsay Barrett,[†,‡] Norma Frizzell,[§] Suzanne R. Thorpe,[§] Mike E Boulton,[‖] John J. McGarvey,[†,‡] and Alan W. Stitt*[,2]

*Centre for Vision Science, School of Biomedical Science, Faculty of Medicine and Health Sciences, Queen's University of Belfast, Belfast, Northern Ireland; [†]School of Chemistry and Chemical Engineering, [‡]Centre for Clinical Raman Microscopy, Queen's University Belfast, Belfast, Northern Ireland; [§]Department of Chemistry and Biochemistry, University of South Carolina, Columbia, South Carolina, USA; and [‖]Department of Ophthalmology and Vision Sciences, the University of Texas Medical Branch, Galveston, Texas, USA

ABSTRACT **The modification of proteins by nonenzymatic glycation leading to accumulation of advanced glycation end products (AGEs) is a well-established phenomenon of aging. In the eyes of elderly patients, these adducts have been observed in retinal pigment epithelium (RPE), particularly within the underlying pentalaminar substrate known as Bruch's membrane. AGEs have also been localized to age-related subcellular deposits (drusen and basal laminar deposits) and are thought to play a pathogenic role in progression of the major sight-threatening condition known as age-related macular degeneration (AMD). The current study has quantified AGEs in Bruch's membrane from postmortem eyes and established age-related correlations. In particular, we investigated the potential of confocal Raman microscopy to identify and quantify AGEs in Bruch's membrane in a nondestructive, analytical fashion. Bruch's membrane and the innermost layers of the underlying choroid (BM-Ch) were dissected from fresh postmortem eye-cups (n=56). AGE adducts were quantified from homogenized tissue using reverse-phase HPLC and GC/MS in combination with immunohistochemistry. For parallel Raman analysis, BM-Ch was flat-mounted on slides and evaluated using a Raman confocal microscope and spectra analyzed by a range of statistical approaches. Quantitative analysis showed that the AGEs pentosidine, carboxymethyllysine (CML), and carboxyethyllysine (CEL) occurred at significantly higher levels in BM-Ch with age (P<0.05–0.01). Defined Raman spectral "fingerprints" were identified for various AGEs and these were observed in the clinical samples using confocal Raman microscopy. The Raman data set successfully modeled AGEs and not only provided quantitative data that compared with conventional analytical approaches, but also provided new and complementary information *via* a nondestructive approach with high spatial resolution. It was shown that the Raman approach could be used to predict chronological age of the clinical samples (P<0.001) and a difference in the Raman spectra between genders was highly significant (P<0.000001). With further development, this Raman-based approach has the potential for noninvasive examination of AGE adducts in living eyes and ultimately to assess their precise pathogenic role in age-related diseases.—Glenn, J. V., Beattie, J. R., Barrett, L., Frizzell, N., Thorpe, S. R., Boulton, M. E., McGarvey, J. J., Stitt, A. W. Confocal Raman microscopy can quantify advanced glycation end product (AGE) modifications in Bruch's membrane leading to accurate, nondestructive prediction of ocular aging. *FASEB J.* 21, 3542–3552 (2007)**

Key Words: RPE · Raman spectroscopy

AGING OF THE RETINA IS CHARACTERIZED by progressive dysfunction of the retinal pigment epithelium (RPE) and its specialized basal lamina, known as Bruch's membrane. Age-related lesions in the outer retina are collectively referred to as early age-related maculopathy (ARM) during which there is no overt visual loss. However, a proportion of patients with ARM will develop geographic atrophy (a confluent wasting of the RPE and choriocapillaris) and/or choroidal neovascularization (CNV), which are associated with photoreceptor damage and represent the two late-stage manifestations of age-related macular degeneration (AMD). This disease can result in severe irreversible loss of

[1] These authors contributed equally to this work.

[2] Correspondence: Centre for Vision Science, School of Biomedical Science, Queen's University Belfast, Royal Victoria Hospital, Belfast BT12 6BA, Northern Ireland. E-mail: a.stitt@qub.ac.uk

doi: 10.1096/fj.06-7896com

0892-6638/07/0021-3542 © FASEB

central vision and remains the leading cause of blindness in the Western world (1).

Characteristic pathology is associated with retinal aging, ARM, and progression to AMD. These changes constitute accumulation of sub-RPE material (drusen and basal laminar deposits) and RPE-associated intracellular pigmentary irregularities, lysosomal dysfunction, and accumulation of lipofuscin granules (2). Concomitantly, Bruch's membrane undergoes increased thickening and reconfiguration of its chemical composition during aging (2, 3). Component collagens in this lamina become progressively cross-linked and show decreased solubility with age, occurring simultaneously with accumulation of granular, membranous, filamentous, and vesicular material and characteristic changes in lipid composition (4). Moreover, an exponential increase in phospholipids, triglycerides, fatty acids, and free cholesterol content of Bruch's membrane from donors >50 years of age has been shown (5), and this may be linked to the development of various forms of extracellular drusen (6).

Inherent in age-related pathology is modification of the ε-amino groups on proteins by advanced glycation chemistry, which has important pathophysiological implications for diabetes and aging (7). So-called advanced glycation end product (AGE) adducts are recognized as important instigators of age-related dysfunction, causing protein cross-linking, reduced solubility, enzymatic dysfunction, and loss of receptor recognition (7). Aging is associated with accumulation of AGEs such as pentosidine, (8), N^{ε}-(carboxymethyl)-lysine (CML), N^{ε}-(carboxyethyl)lysine (CEL), and hydroimidazolone adducts, where they can contribute to pathogenic abnormalities in cells and tissues (9, 10). Immunoreactivity to some of these adducts also occurs with age at the Bruch's membrane-RPE axis (11–14) and within basal lamina deposits from human maculae (15), although the precise contribution of AGEs to outer retinal pathology remains to be elucidated.

In the current study we used conventional specific chemical quantification to assess defined AGE adducts in Bruch's membrane over an age range of postmortem eyes. In parallel, we also used the nondestructive technique of confocal Raman microscopy to quantify AGE-related spectral alterations in Bruch's membrane *ex vivo*. Raman spectroscopic methods analyze the inelastic scattering of photons caused by changes in the vibrational energy of molecules upon excitation with monochromatic light. The light scattered from the sample is collected and split into its different energies, which are then recorded to give a Raman spectrum. Combining Raman spectroscopy with optical microscopy allows acquisition of highly detailed chemical, physical, and biochemical data on a micron scale of spatial resolution without tissue destruction. So far there have been no published characterizations of AGE accumulation using Raman spectroscopy, although the technique has been used to detect diabetes-related changes in vitreous samples from patients with diabetic retinopathy (16), to analyze cataract formation and AGE precursor formation in diabetic lenses (17), and for *in situ* monitoring of macular carotenoid pigments (18, 19). The development of confocal Raman microscopy as a noninvasive, robust method for the valid identification and quantification of AGEs offers considerable diagnostic potential for analysis of these pathogenic agents in ocular tissues.

MATERIALS AND METHODS

Clinical samples

Human donor eyes (n=56; 32–92 years of age) were obtained from patients of various ages and both genders. None of the patients had been diagnosed with AMD, and a range of causes of death were documented. Since this was an aging study, we classified eyes into young (<50 years old, n=8), intermediate (50–70 years, n=27), and old (70+ years, n=21). Eyes were retrieved ~4 h postmortem and immediately placed on ice. The anterior portion of the eye was removed and the RPE layer was brushed off as described previously (20). All methods were carried out in accordance with the tenets of the Declaration of Helsinki for research involving human tissue. In addition, informed consent was obtained from relatives prior to the study and ethical approval was obtained from Research Ethics Committees of all involved institutions.

The posterior segments, with RPE removed, were stored at −80°C. Before use, the samples were thawed on ice in phosphate-buffered saline (PBS), pH 7.4. The retrieved eyecups were then dissected bilaterally and strips of Bruch's membrane-choroid (BM-Ch) adjacent to the macula (1 cm×0.5 cm) were dissected from the remaining eyecup, then frozen and stored at −80°C.

Reference compounds

Model AGEs were prepared by incubating bovine serum albumin (BSA fraction V, Sigma-Aldrich Company Ltd., Dorset, UK, at 10 mg/ml) in 0.5 mol/L glucose solution for 8 wk at 37°C, as described previously (21). CML-BSA and pentosidine were prepared as described (22, 23).

Measurement of AGEs

Dissected BM-Ch were homogenized under liquid nitrogen and protein estimations were conducted using the BCA Protein Assay method (Pierce, Rockford, IL, USA). Pentosidine and CML were quantified using HPLC and GC/MS, respectively, as described previously (24). Briefly, for pentosidine analysis, dissected BM-Ch were reduced with sodium borohydride in sodium borate buffer (pH 9.2), followed by protein precipitation with trichloroacetic acid (TCA). Lipids were extracted from the resuspended protein pellet with ice-cold methanol:ether (3:1), after which reverse-phase HPLC (RP-HPLC) was conducted. Limits of detection and linearity range of the HPLC were 0.025–1.6 pmol (r=0.98). In some cases, a fixed amount of standard pentosidine (0.1–0.4 pmol) was assayed in a "mixing experiment," as described previously (24). Results were expressed as pmol pentosidine/mg protein as calculated from the BCA assay.

GC/MS analysis (n=9) for CML and CEL was carried out on reduced BM-Ch samples processed as outlined above. The GC/MS was conduced as described previously (25) and the AGE concentrations were expressed as mmol/mol lysine. For parallel CML immunohistochemistry, BM-Ch samples were

fixed in 4% (w/v) PFA (Sigma-Aldrich) and processed according to a previously published protocol with slight modifications (26). Briefly paraffin sections were permeabilized using PBS-Tween (0.1%), blocked with 5% normal goat serum (NGS), and stained with polyclonal anti-CML antibody. Some were treated with PBS alone or an IgG rabbit polyclonal (DakoCytomation Ltd., Glostrup, Denmark) as negative and isotype controls. Immunoreactivity was detected with the secondary antibody horseradish peroxidase-conjugated goat anti-rabbit (1:100), then stained with 3-amino-9-ethylcarbazole and chromogen substrate (DakoCytomation). The sections were counterstained with Mayer's hematoxylin (Sigma-Aldrich), mounted in an aqueous mounting medium (DakoCytomation), and visualized by bright-field microscopy (Lucia G/G-F, Nikon, Surrey, UK).

Confocal Raman microscopy

Segments of BM-Ch measuring ~0.5 cm^2 in diameter in the region of the central retina were microdissected from the sclera. With Bruch's membrane uppermost, the samples were placed directly onto extra-white slides (Menzel-Glaser, Braunschweig, Germany) to minimize the non-Raman background from the substrate. All specimens were pretreated in this fashion in preference to the standardized procedure of storage in 4% paraformaldehyde (PFA), which would be expected to introduce artifactual cross-linking of the tissues.

Raman analysis was performed using a Raman confocal microscope (Horiba LabRam HR800; Jobin-Yvon, Villeneuve d'Ascq, France) with 633 nm excitation (20 mW), a ×100 objective, and a slit width of 150 μm. A confocal hole size of 200 μm was used to give a nominal *z* axis resolution of 1.5 μm. An area was selected and 100 spectra (10×10 grid) were accumulated in the 700-1800 cm^{-1} region for 30 s. All spectral acquisition was carried out in Labspec software V4.16 (Jobin-Yvon).

Non-Raman background correction

Raman spectra were obtained for the model AGEs pentosidine, AGE-BSA, and CML-BSA in a cell-free fashion. In common with many other biological systems, a degree of non-Raman background fluorescence was present in the samples studied. These were corrected for in two stages. Principal components analysis (PCA) was initially conducted on the unprocessed Raman data and the dominant non-Raman signals were identified. Any residual Raman signals were subtracted using a chemically equivalent signal that had no significant background. The root mean square best-fit polynomial line (degree=9) was determined for each background in order to obtain a smooth noiseless line approximating the various background shapes within the data set. The linear combination of these backgrounds that gave the most effective background subtraction was calculated in Microsoft Excel (Microsoft Corporation, Redmond, WA, USA).

Any remaining background was removed in Labspec software V4.16 (Jobin-Yvon) using a series of linear extrapolations between adjacent minima within the spectrum. Since there are no common baseline points available for heme and protein, an adaptive method of analysis was employed. Instead of analyzing selected fixed points for baseline determination of samples, the minimum value within a restricted range of Raman shifts was selected, allowing the baseline point to be adjusted according to the spectral shape.

The absolute signal intensity of the Raman signal from any given component of a sample is generally nonreproducible due to a high number of influencing factors including focal position, sample absorbency, laser power, and path length. To standardize the signal, it is necessary to normalize the spectral intensity to an internal standard. In this study, the spectral intensity was normalized by dividing each point by the background-corrected average intensity between 1555 and 1670 cm^{-1} (baseline points at 1500 and 1725 cm^{-1}). This region was chosen in order to include both heme and protein signals.

Statistical analysis

Raman spectral analysis was conducted using The Unscrambler V9.6 (Camo, Trondheim, Norway). PCA was carried out on the full data set to assess the overall signal variation within the data set and identify important spectral signals (27). A multivariate regression technique known as "projection to latent structures" was used to calibrate the Raman signal against the chronological age, gender of the donor, and analytically quantified AGEs. Models were constructed for each reference parameter, then used to predict the levels of those parameters in the remaining data set. Multivariate analysis methods used included PCA and regression methods such as partial least squares (PLS) and discriminant analysis. In all statistical analyses, the spectra were mean-centered and cross validation was used to validate the model.

Statistical analysis of the Raman-predicted results, together with the HPLC and GC/MS data, was performed using Microsoft Excel to calculate mean and standard deviation (SD). Subsequently, a 1-way ANOVA with Bonferroni *post hoc* analysis was conducted using the statistical analysis package SPSS. Data were considered significant at the 95% level ($P<0.05$). A gender comparison was carried out using Student's *t* test (unpaired, unequal variances). As male samples were more numerous, a randomly selected subset was used in this comparison with female samples.

RESULTS

AGEs in Bruch's membrane-choroid complex

Prior to pentosidine analysis, an internal pentosidine model AGE standard was run alongside each individual experiment at 0.404 pmol to confirm elution time (**Fig. 1*C***). A typical chromatogram for Bruch's membrane-choroid specimens from younger patients showed a small peak eluting close to the retention time for authentic pentosidine (Fig. 1*Ai, Aii*, depicting a confirmatory mixing experiment using synthetic pentosidine to "spike" the sample and validate the pentosidine specific nature of the peak by increasing peak height). Chromatograms from older donors (~70 years) typically showed a larger pentosidine peak compared with young specimens (Fig. 1*Bi, ii*). In terms of grouped analysis of pentosidine in BM-Ch, there was a doubling in pentosidine content of samples from groups aged 50–70 years compared with young samples (<50 years) ($P<0.01$) (Fig. 1*D*). The increase in pentosidine with age was >4-fold with the oldest age group (>70 years) ($P<0.005$).

CML immunoreactivity occurred at Bruch's membrane and also deeper within the choroid. CML inten-

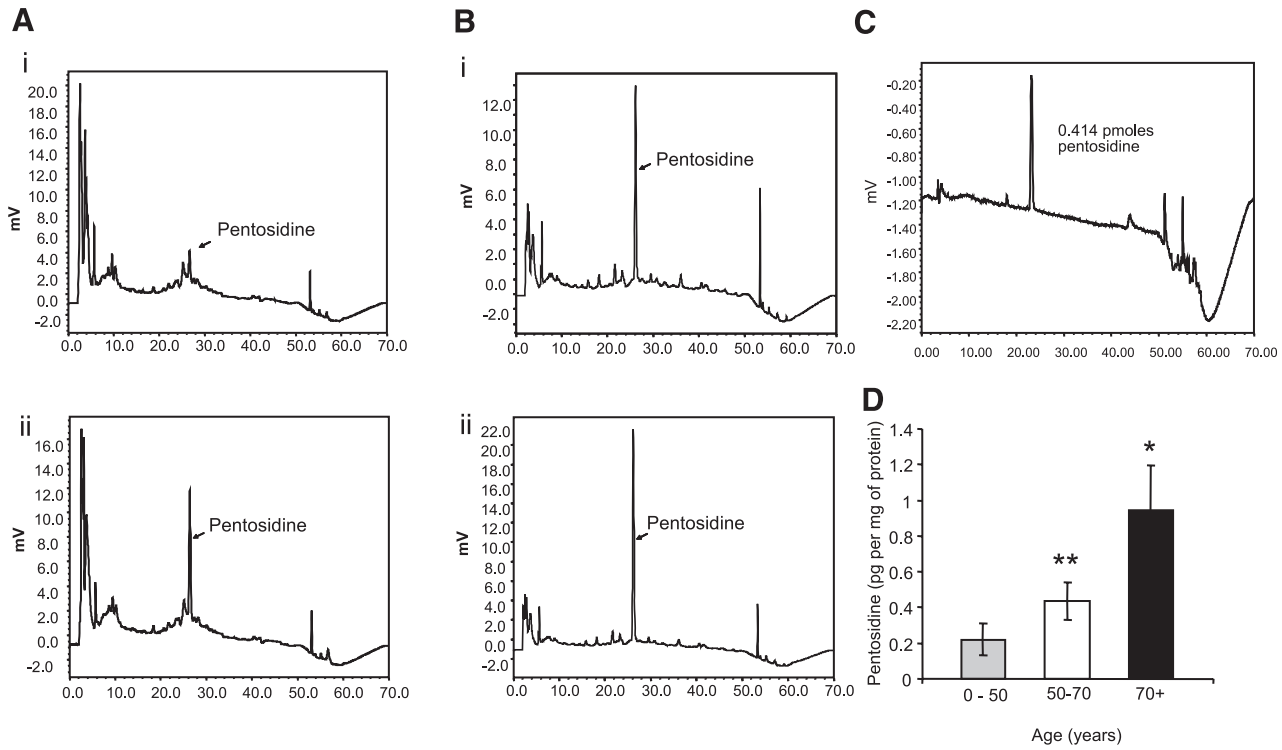

Figure 1. Pentosidine accumulation in Bruch's membrane choroid. HPLC analysis of pentosidine in human BM-Ch. *A, B)* Representative elution profiles of BM-Ch are shown. A sample chromatograph from a 41-year-old female shows a small pentosidine peak (*Ai*) that is confirmed as the profile characteristic of this AGE when the sample is coinjected with a pentosidine standard (*Aii*). A BM-Ch extract from an older patient produces a chromatograph with elevated levels of pentosidine (*Bi*), confirming this as an AGE-specific profile by coinjection of a standard with the clinical sample (*Bii*). *C)* HPLC analysis revealed a characteristic profile from a standard injection series, indicating the peaks assigned to the pentosidine standard (0.414 pmol) and the additional argpyrimidine standard (50 pmol). Within the constraints of the current analysis, argpyrimidine was not found at significant levels in any clinical material. *D)* Analysis of all the clinical samples demonstrated there was an increase in pentosidine, with age. There were significant increases in the 70+ age group (*$P<0.01$) compared with the other age groups and with a highly significant difference between the 0–50 and 50–70 age groups (**$P<0.005$).

sity was increased in sections from older patients (compare **Fig. 2*A*** with Fig. 2*B*), whereas isotype controls showed negative staining (Fig. 2*C*). Quantification of CML using GC/MS demonstrated that older patients had significantly higher levels of this adduct in BM-Ch ($P<0.05$) (Fig. 2*D*). GC/MS studies also quantified the related adduct CEL, but differences were not statistically significant (Fig. 2*D*).

Confocal Raman microscopy of AGEs

Prior to analysis of tissue samples, the Raman signals of a generalized AGE-albumin and an albumin specifically modified by CML were compared with native albumin, with the difference between the Raman signals for the modified and unmodified albumins reflecting the Raman band shape of AGE adducts (**Fig. 3*i–iv***). The Raman signal of pure pentosidine was also obtained for reference (Fig. 3*v*) The Raman signal for the undefined range of adducts formed during the incubation of albumin in glucose showed a doublet of bands at 400 and 540 cm^{-1} as well as a triplet of bands at 880, 980, and 1090 cm^{-1}. Although CML showed a band shape superficially similar to that of the undefined AGE adduct, significant shifts in band positions were evident (Fig. 3*iv*). The CML spectrum contained a doublet at 510 and 565 cm^{-1} and bands at 860, 930, 1000, 1065, and 1130 cm^{-1}. In contrast, the spectrum of pentosidine (Fig. 3*v*) showed a much greater number of narrower bands covering a wider range of the spectrum. For further investigation, the 700-1800 cm^{-1} region of the spectrum was chosen for clinical sample analysis.

Confocal Raman microscopy of Bruch's membrane

For Raman spectroscopic analysis, all measurements on BM-Ch were made at a maximum depth of 4 μm. This depth was chosen after pilot studies in which deeper optical sections resulted in Raman scattering from within the choroid. It was also found that high melanin content in the choroid swamped the Raman signal from overlying Bruch's membrane; thus, all confocal measurements were taken at a defined depth.

PCA of the Raman data revealed significant spectral signals (**Fig. 4** and supporting information for the first 18 chemically significant principal components) with associated band assignments (**Table 1**). The Raman signal was dominated by spectral features attributable to a protein, with a significantly high proportion of

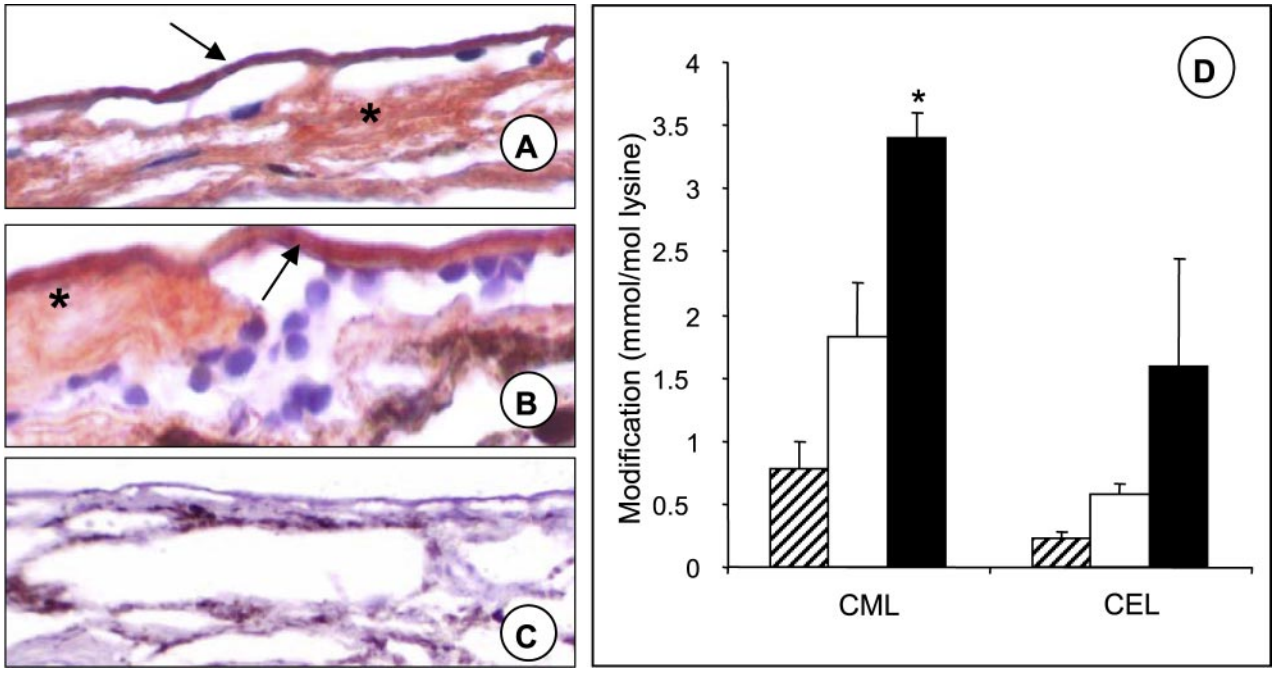

Figure 2. Immunolocalization and quantification of AGEs in Bruch's membrane. CML immunoreactivity was determined in sections of Bruch's membrane–choroid complex. Representative sections are shown from a 60-year-old (*A*) and an 86-year-old donor (*B*). In both cases the antibody localized CML to Bruch's membrane with greatest intensity (arrow). There was also significant deposition in the extracellular matrix of the choroid (*). Isotype (*C*) or secondary omission controls showed no evidence of staining (original magnification: ×200). CML and CEL were quantified in Bruch's membrane–choroid complex by GC-MS from donors aged 0–50 years (hatched bars), 51–79 years (white bars), and > 80 years (black bars) (*D*). There was a statistically significant increase in CML in the oldest compared with the youngest cohort, but no difference among the cohorts in CEL. $*P < 0.05$.

proline and hydroxyproline and a random coil secondary structure (Fig. 4*ii*). Signals characteristic of heme and a spectral signal similar to that of the undefined AGE adducts identified above, previously unreported in the literature, were also dominant in the data set (Figs. 4*i, iii*). In Bruch's membrane, this AGE signal (arrowed in Fig. 4*iii*) was observed in association with collagen and heme; when these spectra were subtracted, a signal closely matching that of a combination of arginine and lysine remained (asterisked in Fig. 4*iii*). The variation in the heme signal was significantly greater (a factor of 10) than variation in any of the other constituents, accounting for 71% of the total variation within the unprocessed data set compared with 7% of the variation explained by the second component. This dominant signal was found to be unrelated to the parameters of interest here (*i.e.*, donor age and pentosidine levels and gender; $R^2<0.1$; see supporting information), but

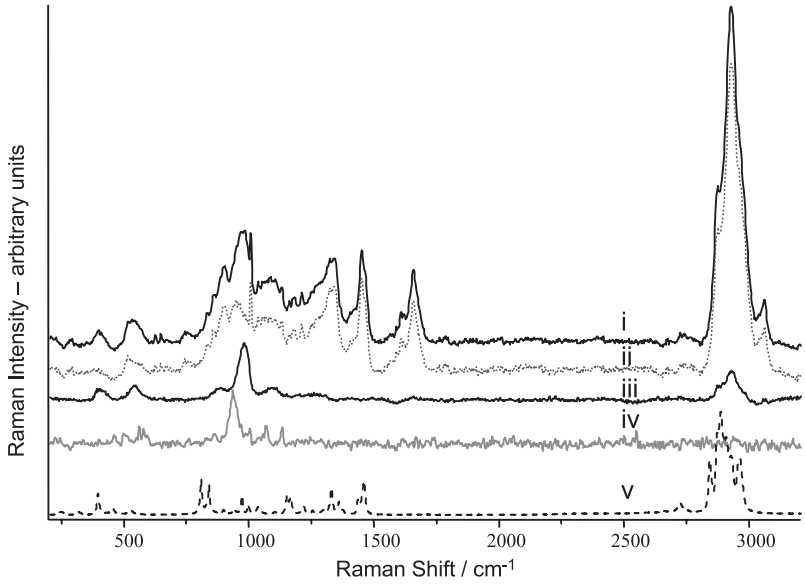

Figure 3. Raman analysis of AGEs. Comparisons were made between the Raman signals obtained from *i)* AGE-modified BSA and *ii)* unmodified BSA. The difference between the two signals (subtraction spectrum, *iii)* corresponds to the signal from AGE modifications. *iv)* Equivalent Raman subtraction spectrum of CML-BSA that shows marked superficial similarly to AGE-BSA spectrum shown, but significant band shifts. *v)* Raman signal obtained from pure pentosidine.

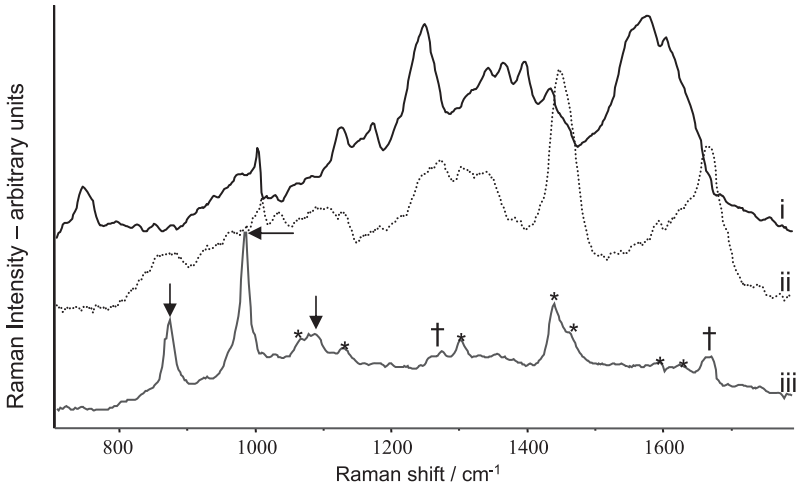

Figure 4. Raman analysis of Bruch's membrane. The three dominant Raman spectral signals identified using PCA. These were found to closely match the signal for *i)* heme, *ii)* collagen, *iii)* AGE (arrow), arginine/lysine (*), and peptide bonds (†). These spectra are the average of the extreme PC scores for selected chemically significant components. *i–iii*) A small contribution from collagen and from heme and collagen signals, respectively, was subtracted for clarity. Additional information on further PC scores is available on-line.

its influence was minimized by normalizing the spectra in such a way that the variation due to heme was reduced within the data set. Although the least squares regression correlation between the heme signal and these parameters was poor, there was a significant increase in the heme signal in females *vs.* males ($P<0.05$) and in those >60 years old compared with those under 60 years old ($P<0.01$) (**Table 2**).

AGEs in Bruch's membrane and Raman comparative analysis

PLS regression analysis showed a positive correlation for pentosidine concentration as determined by HPLC *vs.* that determined by Raman analysis (**Fig. 5*A***), although the correlation did not work effectively for both sexes simultaneously and required separate models to be created for the male and female samples to provide optimum model performance (**Table 3**). Raman analysis of pentosidine showed significantly greater levels in patients older than 60 years compared with patients under 60 ($P<0.05$, Fig. 5*B*). Notably, males showed ~3-fold the level of this AGE compared with females for both the Raman-predicted ($P<0.001$) and HPLC-measured data sets ($P<0.05$), whereas the level of pentosidine was 2.5-fold higher in males older than 60 than in those under 60 ($P<0.05$) (Table 2). Positive contributions to the regression coefficients selected by the uncertainty test as being the most correlated with pentosidine concentration (**Fig. 6*Aii***) all match band positions that occur within the Raman signal of pure pentosidine (Fig. 6*Ai*).

As with pentosidine, validation PLS regression analysis for Raman spectra from CML and CEL revealed a positive correlation between GC/MS analysis and Raman spectroscopy (Fig. 5*C* and Table 3) as well as a close match between the Raman signal of the adduct and the regression coefficients used to predict the quantity of that adduct in Bruch's membrane (Fig. 6*B*). The Raman-predicted CML level also showed a significant change with age and significantly elevated levels in females compared with males ($P<0.05$ and 0.0001, respectively). The Raman-predicted CEL levels showed no significant variation with age or gender (Table 2).

Overall analysis of the Raman data set confirmed the gender and age differences within the BM-Ch samples, with PLS regression against gender and age group revealing highly significant differences in the Raman signals of male *vs.* female and under 60 *vs.* over 60 (**Fig. 7*A, B***, $P<0.00001$ in each case). The regression coefficients used to separate the sexes are shown in Fig. 7*C* and closely match those of the AGE adduct in Fig. 4*iii*.

DISCUSSION

AGE adducts accumulate on long-lived extracellular proteins with age (28), and further knowledge of these modifications in Bruch's membrane contributes to our understanding about the age-related pathophysiology of the RPE and perhaps progression to AMD. In this study we have demonstrated the age-dependent accumulation of defined AGE adducts in human BM-Ch. The study has also established the utility of confocal Raman microscopy for nondestructive analysis of age-related changes and quantitative evaluation of pathogenic protein modifications in Bruch's membrane.

As an "archetypical" AGE cross-link, pentosidine was previously localized to Bruch's membrane using immunohistochemistry (13, 29), and suggestions that levels are increased in aging are confirmed by the quantitative approach of the current study. It is also worth noting that pentosidine may be present at relatively low concentrations in tissues (30) and therefore may only reflect the "tip of the iceberg" for outer retinal AGE accumulation. We observed that CML was also increased in aging Bruch's membrane, and this evidence concurs with documented findings in aged human skin collagen (28, 31), lens (23), and a qualitative study showing the presence of this AGE in RPE and drusen from patients with wet AMD (14).

The accumulation of AGEs in Bruch's membrane perhaps is not surprising due to the environmental conditions and metabolic demands of the outer retina,

TABLE 1. *Raman assignments of selected bands in the 700-1800 cm^{-1} region from Bruch's membrane*

Raman Shift/cm-1	Assignment	Comments
740	heme	
750	heme, collagen	arg, hpro
803	pentosidine	
830	collagen	Pro
838	pentosidine	
850	collagen	hpro, arg
860	collagen	arg, lys
875	collagen	Pro
880	AGE	
890	collagen, fat	terminal C—C bonds
910	collagen	Pro
940	heme, collagen	C—C bonds, α-helix conformation in proteins
965	collagen	Arg
970	heme, pentosidine	
980	AGE	
995	heme, collagen, pentosidine	arg, pro
1010–20	collagen	arg, lys
1030	collagen	
1050	collagen	arg, lys, pro
1060	fat, collagen	C—C bonds, arg
1080–90	collagen, AGE, fat	C—C bonds in non-linear molecules, arg, hpro
1125	heme, collagen, fat	C—C bonds
1136	collagen	arg, lys
1150	pentosidine	
1160	collagen, pentosidine	lys, pro
1180	collagen	Hpro
1215	pentosidine	
1250	heme, collagen	amide III (peptide bonds)
1270	fat	═C-H bonds
1315	collagen	arg, hpro, lys
1300,26,60	pentosidine	
1340,65,95	heme	porphyrin group, sensitive to redox reactions
1400–1500	heme, collagen, fat	CH2 groups
1430,1455	pentosidine	
1435	collagen	arg, lys
1460	collagen	arg, lys
1527	collagen	Arg
1545,75,1610	heme	porphyrin group, sensitive to redox reactions
1550	collagen	Pro
1575	collagen	Lys
1585	collagen	Arg
1605	collagen	hpro, pro
1620	collagen	arg, lys, pro
1650–80	collagen, fat	amide I (peptide bonds), C═C

TABLE 2. *Statistical significance of comparing Raman predicted, HPLC and GCMS measured parameters with gender and age groups (<60 vs. >60)*[a]

	$P <$ (gender)	High	$P <$ (age group)	High
Raman heme signal	0.05	F	0.01	O
Raman-predicted pentosidine	0.001	M	0.05	O
HPLC-measured pentosidine	0.05	M	0.05	O
Raman-predicted CML	0.0001	F	0.05	O
GCMS-measured CML	n.a.		0.05	O
Raman-predicted CEL	n.s.		n.s.	
GCMS-measured CEL	n.a.		n.s.	
Overall Raman signal	0.00001	F	0.00001	O

[a] The groups showing elevated levels are shown, with M = male, F = female, O = >60. Gender comparison of CML and CEL GCMS data could not be made due to the small number of female donors measured. n.a., not applicable; n.s. not significant; $P > 0.05$.

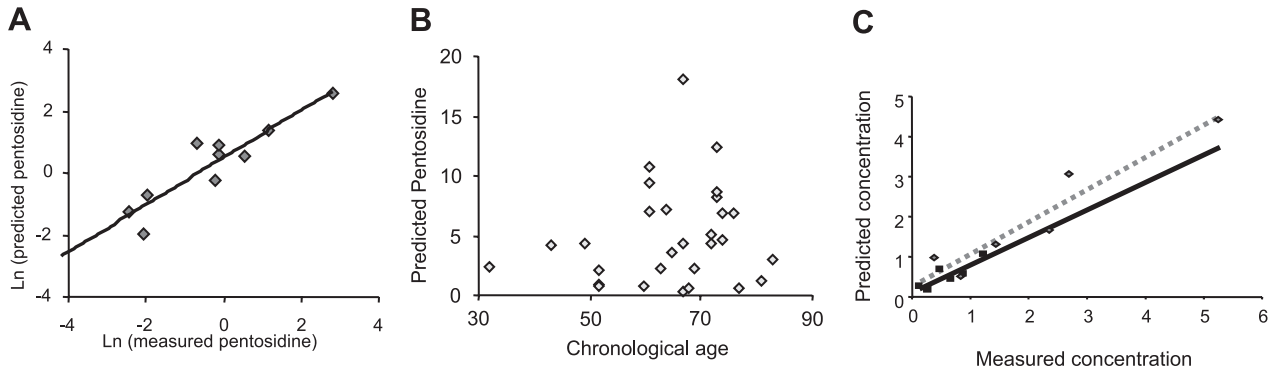

Figure 5. Raman analysis of pentosidine in Bruch's membrane. *A)* PLS regression plot for the prediction of pentosidine concentration from Raman spectra of Bruch's membrane. *B)* Plot of predicted pentosidine concentration against age. The difference between samples over 60 and under 60 is significant ($P<0.05$). *C)* Validation PLS regression plot predicts the concentration of CML (dotted line) and CEL (solid line) adducts in Bruch's membrane using Raman microscopy.

which include supranormal mitochondrial-derived ATP (oxidative phosphorylation activity), high concentrations of unsaturated lipids, and accompanying high oxygen/glucose from the underlying choroid (32). These factors that have the potential to generate superoxide, combined with the longevity of many extracellular proteins, leave Bruch's membrane susceptible to AGE accumulation, since adducts are removed only when the protein itself is degraded (33). The functional significance of these adducts in Bruch's membrane resides in their potential to affect permeability and hydraulic conductivity, which are known to diminish with age (34). Thus, AGE accumulation can be regarded as a likely pathogenic factor when considering age-related changes to Bruch's membrane such as reduced permeability, enhanced rigidity, and thickening (3, 34, 35). Such extracellular matrix defects had previously been attributed to AGE-cross-linking in other systems (36). Indeed, recent reports have highlighted the importance of increased protein cross-linking with age in "ocular rigidity" (37), a phenomenon that also shows a higher incidence in AMD patients (38). The current study also highlights the potential for therapeutic agents that can prevent (39) or even break established AGE-protein adducts (40) in the context of retinal aging.

Quantitative AGE analysis is inherently destructive and fails to differentiate between regional variations in adduct levels in complex tissues. The nondestructive confocal microscopy approach combined with Raman spectroscopic analysis employed here is advantageous because it simultaneously measures multiple chemical components and allows further study of the tissues under examination. This is inherently useful, as Bruch's membrane is intimately associated with the underlying choriocapillaris and obtaining pure extracts of this pentalaminar structure to date demands pulsed excimer laser microdissection approaches (41). Indeed, we have already shown that a layered structure like the neural retina can be systematically analyzed using this confocal Raman approach and that dodecahexaenoic acid, cytochrome *c*, DNA, and other proteins can be detected and spatially resolved within the neural layers (42, 43).

AGE spectral signatures can be identified in Bruch's membrane using confocal Raman microscopy. Detailed analysis has identified 18 chemically significant principal components, each of which contains contributions from two biochemical entities (Supplemental Fig. 1). The dominant Raman signal in Bruch's membrane showed intensity at positions typical of random coil secondary structure and the amino acid residues proline and hydroxyproline; this correlated well with collagens that comprise Bruch's membrane. The occurrence of the heme signal was unexpected within Bruch's membrane. Due to the confocal conditions in

TABLE 3. *Results of PLS regression analysis of Raman spectra of Bruch's membrane with various parameters*

	R^2	SEP[a]	SEE[b]	No. factors	No. donors
Age	0.630	5.17	5.50	10	41
Age male	0.644	4.84	3.83	3	30
Age female	0.686	7.18	7.89	6	11
Pentosidine	0.487	3.89	4.55	9	33
Pentosidine male	0.907	0.84	1.603	7	16
Pentosidine female	0.972	0.17	0.45	4	5
CML	0.906	0.49	0.89	3	6
CEL	0.751	0.15	0.19	5	6

[a]Standard error of prediction. [b]Standard error of estimate.

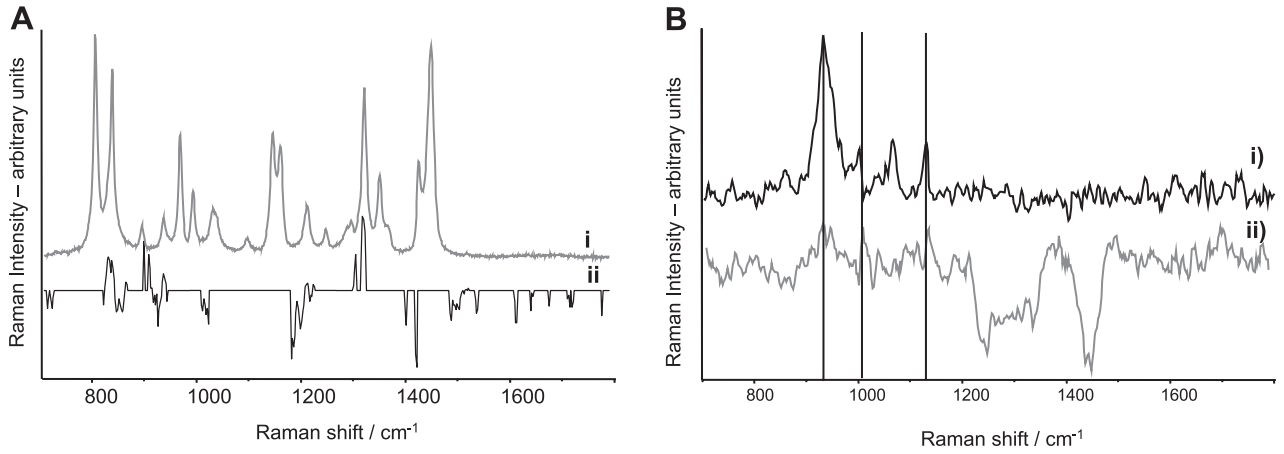

Figure 6. Age prediction using Raman spectral analysis of AGEs. *Ai)* Raman spectrum of pentosidine compared with *ii)* the regression coefficients selected by the uncertainty test as most correlated with pentosidine concentration. The bands of the Raman signal that positively contribute to the regression coefficients match bands that occur in the spectrum of pentosidine. *B)* Illustration of the close match between *i)* the Raman signal of the CML adduct and *ii)* the regression coefficients used to predict the quantity of that adduct in Bruch's membrane

the current Raman studies, the possibility of interference from the choriocapillaris can be ruled out, although there may be blood products lodged within the extracellular matrix.

There have been few studies of AGEs using Raman spectroscopy. Sebag *et al.* used a nonmicroscopy-based approach to show Raman spectral changes in the human vitreous that were attributed to AGEs (16). The current investigation has demonstrated that Raman spectral evaluation of defined AGEs is a valid approach to quantify these adducts. Moreover, measuring AGEs by confocal Raman microscopy can accurately predict chronological age in human Bruch's membrane. This is a significant finding, consistent with other studies showing that AGEs in long-lived proteins correlate with aging in humans and animals (44, 45). Some caution is warranted, however, as there are several potentially confounding factors in the current study. Although we were able to exclude patients with diagnosed diabetes and/or renal dysfunction, it is possible that some samples were from individuals with nondiagnosed type 2 diabetes and/or a degree of kidney disease. It is not known whether diabetic patients have higher AGEs in Bruch's membrane, but there is ample evidence that these adducts are elevated in the skin collagen and lens of such individuals (46) and in those undergoing hemodialysis (47). It is possible that these unknowns could lead to elevated AGE levels in some samples. In addition, no information was available concerning possible smoking history, which is also known to increase AGE levels in patients (48) and is linked to AMD (49). Further Raman studies of well-characterized patient groups with ARM, AMD, and nondiseased age-matched controls are ongoing in our laboratory.

The identification of a gender difference in Bruch's membrane AGEs, as identified by Raman spectroscopy, is interesting, especially considering the higher incidence of ARM and AMD in females (50). The underlying reason for this imbalance is unclear, although a study in type 2 diabetics has indicated that gender was

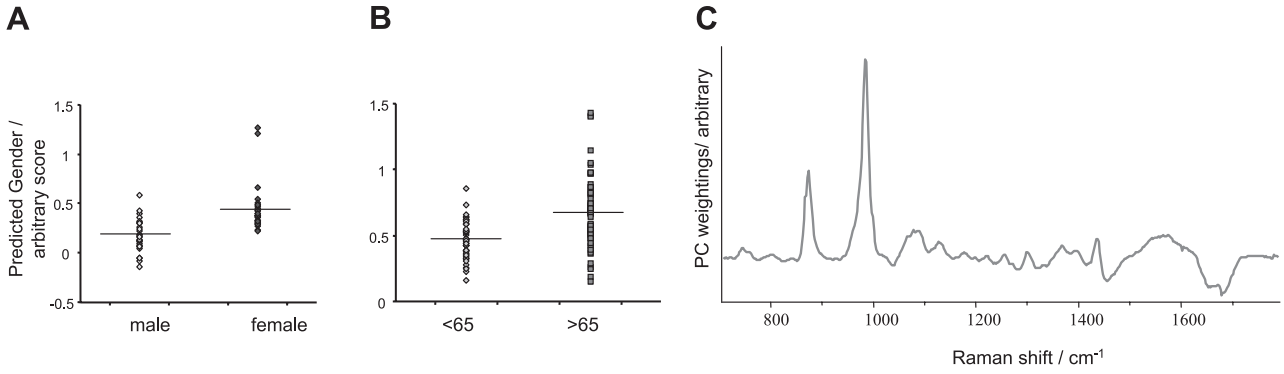

Figure 7. Gender differences in AGEs within Bruch's membrane during aging. *A)* Gender score (0=male, 1=female) and *B)* age score (0=under 60, 1=over 60) predicted from the Raman signal of human donor Bruch's membranes. The predicted score is significantly different between the sexes and between age groups ($P<0.00001$). The average age of each gender and the gender composition of the two age groups are not significantly different ($P>0.05$). *C)* Most significant PC used to separate the genders and the age groups. The positive bands match the Raman signals of AGE and heme and the negative bands match those of collagen.

a significant independent predictive factor for AGEs, with women having significantly elevated levels even when adjusting for discrepancies in hemoglobin levels (51). Gender differences in various AGE adducts have not always been uncovered in clinical studies (47), and this area requires further study.

The present investigation provides a preliminary demonstration of the potential of Raman microscopy as a robust, nondestructive method for quantifying AGE accumulation in ocular tissues. The use of Raman spectroscopy to evaluate the extent of aging in specific tissues as well as to evaluate the pathogenicity of corresponding protein modifications represents an important step toward noninvasive evaluation of the retina. Indeed, the intraocular Raman approach has been reported for *in situ* monitoring of macular carotenoid pigments (18, 19). The results accrued to this juncture already provide some demonstration that chronological age and gender differences in human specimens can be reliably predicted *via* Raman measurements of AGEs. The assembly of a more comprehensive library of Raman spectra for AGE adducts is in progress, but even at this stage our findings have the potential to significantly extend earlier studies by conventional analytical techniques that correlate AGE levels with aging in humans and appropriate animal models. Moreover, tracking pathogenic AGE adducts in the living eye using confocal Raman microscopy could ultimately provide unique and useful diagnostic information about patient susceptibility to a range of important diseases such as AMD, cataract formation, posterior vitreal detachment, and diabetic retinopathy. FJ

The authors would like to acknowledge financial support from The Medical Research Council (MRC) (grant no. G0600053), The Wellcome Trust (WT066193), The Biotechnology and Biological Sciences Research Council (BBSRC) (JREI 18471), The Research and Development Office (NI), The Belfast Association for the Blind, Insight: The Trust for the Visually Impaired, and USPHS grant DK19971 (MERIT). The authors also thank the Bristol Eye Bank for their donation of clinical material and provision of AMD positive paraffin-embedded tissues essential for this study. J.J.M. thanks the Leverhulme Trust for the award of an Emeritus Research Fellowship (EM/2006/0049).

REFERENCES

1. Kulkarni, A. D., and Kuppermann, B. D. (2005) Wet age-related macular degeneration. *Adv. Drug. Deliv. Rev.* **57,** 1994–2009
2. Zarbin, M. A. (2004) Current concepts in the pathogenesis of age-related macular degeneration. *Arch. Ophthalmol.* **122,** 598–614
3. Okubo, A., Rosa, R. H., Jr., Bunce, C. V., Alexander, R. A., Fan, J. T., Bird, A. C., and Luthert, P. J. (1999) The relationships of age changes in retinal pigment epithelium and Bruch's membrane. *Invest. Ophthalmol. Vis. Sci.* **40,** 443–449
4. Karwatowski, W. S., Jeffries, T. E., Duance, V. C., Albon, J., Bailey, A. J., and Easty, D. L. (1995) Preparation of Bruch's membrane and analysis of the age-related changes in the structural collagens. *Br. J. Ophthalmol.* **79,** 944–952
5. Sheraidah, G., Steinmetz, R., Maguire, J., Pauleikhoff, D., Marshall, J., and Bird, A. C. (1993) Correlation between lipids extracted from Bruch's membrane and age. *Ophthalmology* **100,** 47–51
6. Coffey, A. J., and Brownstein, S. (1986) The prevalence of macular drusen in postmortem eyes. *Am. J. Ophthalmol.* **102,** 164–171
7. Baynes, J. W. (2001) The role of AGEs in aging: causation or correlation. *Exp. Gerontol.* **36,** 1527–1537
8. Sell, D. R., and Monnier, V. M. (2005) Ornithine is a novel amino acid and a marker of arginine damage by oxoaldehydes in senescent proteins. *Ann. N. Y. Acad. Sci.* **1043,** 118–128
9. Thorpe, S. R., and Baynes, J. W. (2003) Maillard reaction products in tissue proteins: new products and new perspectives. *Amino Acids* **25,** 275–281
10. Thornalley, P. J., Langborg, A., and Minhas, H. S. (1999) Formation of glyoxal, methylglyoxal and 3-deoxyglucosone in the glycation of proteins by glucose. *Biochem. J.* 344. Pt. **1,** 109–116
11. Schutt, F., Bergmann, M., Holz, F. G., and Kopitz, J. (2003) Proteins modified by malondialdehyde, 4-hydroxynonenal, or advanced glycation end products in lipofuscin of human retinal pigment epithelium. *Invest. Ophthalmol. Vis. Sci.* **44,** 3663–3668
12. Howes, K. A., Liu, Y., Dunaief, J. L., Milam, A., Frederick, J. M., Marks, A., and Baehr, W. (2004) Receptor for advanced glycation end products and age-related macular degeneration. *Invest. Ophthalmol. Vis. Sci.* **45,** 3713–3720
13. Handa, J. T., Verzijl, N., Matsunaga, H., Aotaki-Keen, A., Lutty, G. A., te Koppele, J. M., Miyata, T., and Hjelmeland, L. M. (1999) Increase in the advanced glycation end product pentosidine in Bruch's membrane with age. *Invest. Ophthalmol. Vis. Sci.* **40,** 775–779
14. Ishibashi, T., Murata, T., Hangai, M., Nagai, R., Horiuchi, S., Lopez, P. F., Hinton, D. R., and Ryan, S. J. (1998) Advanced glycation end products in age-related macular degeneration. *Arch. Ophthalmol.* **116,** 1629–1632
15. Yamada, Y., Ishibashi, K., Bhutto, I. A., Tian, J., Lutty, G. A., and Handa, J. T. (2006) The expression of advanced glycation endproduct receptors in RPE cells associated with basal deposits in human maculas. *Exp. Eye Res.* **82,** 840–848
16. Sebag, J., Nie, S., Reiser, K., Charles, M. A., and Yu, N. T. (1994) Raman spectroscopy of human vitreous in proliferative diabetic retinopathy. *Invest. Ophthalmol. Vis. Sci.* **35,** 2976–2980
17. Furić K, Mohaček-Grošev, V., and Hadžija, M. (2005) Development of cataract caused by diabetes mellitus: Raman study. *J. Mol. Struct.* **744-747,** 169–177
18. Bernstein, P. S., Zhao, D. Y., Sharifzadeh, M., Ermakov, I. V., and Gellermann, W. (2004) Resonance Raman measurement of macular carotenoids in the living human eye. *Arch. Biochem. Biophys.* **430,** 163–169
19. Shih, S., Weng, Y. M., Chen, S., Huang, S. L., Huang, C. H., and Chen, W. (2003) FT-Raman spectroscopic investigation of lens proteins of tilapia treated with dietary vitamin E. *Arch. Biochem. Biophys.* **420,** 79–86
20. Rozanowska, M., Jarvis-Evans, J., Korytowski, W., Boulton, M. E., Burke, J. M., and Sarna, T. (1995) Blue light-induced reactivity of retinal age pigment. In vitro generation of oxygen-reactive species. *J. Biol. Chem.* **270,** 18825–18830
21. Stitt, A. W., Li, Y. M., Gardiner, T. A., Bucala, R., Archer, D. B., and Vlassara, H. (1997) Advanced glycation end products (AGEs) co-localize with AGE receptors in the retinal vasculature of diabetic and of AGE-infused rats. *Am. J. Pathol.* **150,** 523–531
22. Wells-Knecht, M. C., Thorpe, S. R., and Baynes, J. W. (1995) Pathways of formation of glycoxidation products during glycation of collagen. *Biochemistry* **34,** 15134–15141
23. Ahmed, M. U., Brinkmann Frye, E., Degenhardt, T. P., Thorpe, S. R., and Baynes, J. W. (1997) N-epsilon-(carboxyethyl)lysine, a product of the chemical modification of proteins by methylglyoxal, increases with age in human lens proteins. *Biochem. J.* **324,** 565–570
24. Degenhardt, T. P., Grass, L., Reddy, S., Thorpe, S. R., Diamandis, E. P., and Baynes, J. W. (1997) Technical note. The serum concentration of the advanced glycation end-product N epsilon-(carboxymethyl)lysine is increased in uremia. *Kidney Int.* **52,** 1064–1067
25. Dunn, J. A., McCance, D. R., Thorpe, S. R., Lyons, T. J., and Baynes, J. W. (1991) Age-dependent accumulation of N epsilon-

(carboxymethyl)lysine and N epsilon-(carboxymethyl)hydroxylysine in human skin collagen. *Biochemistry* **30,** 1205–1210
26. Stitt, A., Gardiner, T. A., Anderson, N. L., Canning, P., Frizzell, N., Duffy, N., Boyle, C., Januszewski, A. S., Chachich, M., Baynes, J. W., and Thorpe, S. R. (2002) The AGE inhibitor pyridoxamine inhibits development of retinopathy in experimental diabetes. *Diabetes* **51,** 2826–2832
27. Williams, P., and Norris, K., eds (2001) *Near-Infrared Technology in the Agricultural and Food Industries*, AACC Press, St. Paul, MN
28. Sell, D. R., and Monnier, V. M. (2004) Conversion of arginine into ornithine by advanced glycation in senescent human collagen and lens crystallins. *J. Biol. Chem.* **279,** 54173–54184
29. Farboud, B., Aotaki-Keen, A., Miyata, T., Hjelmeland, L. M., and Handa, J. T. (1999) Development of a polyclonal antibody with broad epitope specificity for advanced glycation endproducts and localization of these epitopes in Bruch's membrane of the aging eye. *Mol. Vis.* **5,** 11
30. Lyons, T. J., Silvestri, G., Dunn, J. A., Dyer, D. G., and Baynes, J. W. (1991) Role of glycation in modification of lens crystallins in diabetic and nondiabetic senile cataracts. *Diabetes* **40,** 1010–1015
31. Dyer, D. G., Dunn, J. A., Thorpe, S. R., Bailie, K. E., Lyons, T. J., McCance, D. R., and Baynes, J. W. (1993) Accumulation of Maillard reaction products in skin collagen in diabetes and aging. *J. Clin. Invest.* **91,** 2463–2469
32. Yu, D. Y., and Cringle, S. J. (2001) Oxygen distribution and consumption within the retina in vascularised and avascular retinas and in animal models of retinal disease. *Prog. Retin. Eye. Res.* **20,** 175–208
33. Verzijl, N., DeGroot, J., Thorpe, S. R., Bank, R. A., Shaw, J. N., Lyons, T. J., Bijlsma, J. W., Lafeber, F. P., Baynes, J. W., and TeKoppele, J. M. (2000) Effect of collagen turnover on the accumulation of advanced glycation end products. *J. Biol. Chem.* **275,** 39027–39031
34. Moore, D. J., Hussain, A. A., and Marshall, J. (1995) Age-related variation in the hydraulic conductivity of Bruch's membrane. *Invest. Ophthalmol. Vis. Sci.* **36,** 1290–1297
35. Ishibashi, T., Sorgente, N., Patterson, R., and Ryan, S. J. (1986) Aging changes in Bruch's membrane of monkeys: an electron microscopic study. *Ophthalmologica* **192,** 179–190
36. Verzijl, N., DeGroot, J., Ben, Z. C., Brau-Benjamin, O., Maroudas, A., Bank, R. A., Mizrahi, J., Schalkwijk, C. G., Thorpe, S. R., Baynes, J. W., *et al.* (2002) Crosslinking by advanced glycation end products increases the stiffness of the collagen network in human articular cartilage: a possible mechanism through which age is a risk factor for osteoarthritis. *Arthritis Rheum.* **46,** 114–123
37. Pallikaris, I. G., Kymionis, G. D., Ginis, H. S., Kounis, G. A., and Tsilimbaris, M. K. (2005) Ocular rigidity in living human eyes. *Invest. Ophthalmol. Vis. Sci.* **46,** 409–414
38. Pallikaris, I. G., Kymionis, G. D., Ginis, H. S., Kounis, G. A., Christodoulakis, E., and Tsilimbaris, M. K. (2006) Ocular rigidity in patients with age-related macular degeneration. *Am. J. Ophthalmol.* **141,** 611–615
39. Stitt, A. W., McGoldrick, C., Rice-McCaldin, A., McCance, D. R., Glenn, J. V., Hsu, D. K., Liu, F. T., Thorpe, S. R., and Gardiner, T. A. (2005) Impaired retinal angiogenesis in diabetes: role of advanced glycation end products and galectin-3. *Diabetes* **54,** 785–794
40. Wolffenbuttel, B. H., Boulanger, C. M., Crijns, F. R., Huijberts, M. S., Poitevin, P., Swennen, G. N., Vasan, S., Egan, J. J., Ulrich, P., Cerami, A., and Levy, B. I. (1998) Breakers of advanced glycation end products restore large artery properties in experimental diabetes. *Proc. Natl. Acad. Sci. U. S. A.* **95,** 4630–4634
41. Starita, C., Hussain, A. A., Patmore, A., and Marshall, J. (1997) Localization of the site of major resistance to fluid transport in Bruch's membrane. *Invest. Ophthalmol. Vis. Sci.* **38,** 762–767
42. Beattie, J. R., Brockbank, S., McGarvey, J. J., and Curry, W. J. (2005) Effect of excitation wavelength on the Raman spectroscopy of the porcine photoreceptor layer from the area centralis. *Mol. Vision* **11,** 825–832
43. Beattie, J. R., Brockbank, S., McGarvey, J. J., and Curry, W. J. (2007) Raman Microscopy of porcine inner retinal layers from the area centralis. *Mol. Vision* In press
44. Sell, D. R., Kleinman, N. R., and Monnier, V. M. (2000) Longitudinal determination of skin collagen glycation and glycoxidation rates predicts early death in C57BL/6NNIA mice. *FASEB J.* **14,** 145–156
45. Verzijl, N., DeGroot, J., Oldehinkel, E., Bank, R. A., Thorpe, S. R., Baynes, J. W., Bayliss, M. T., Bijlsma, J. W., Lafeber, F. P., and Tekoppele, J. M. (2000) Age-related accumulation of Maillard reaction products in human articular cartilage collagen. *Biochem. J.* **350,** 381–387
46. Genuth, S., Sun, W., Cleary, P., Sell, D. R., Dahms, W., Malone, J., Sivitz, W., and Monnier, V. M. (2005) Glycation and carboxymethyllysine levels in skin collagen predict the risk of future 10-year progression of diabetic retinopathy and nephropathy in the diabetes control and complications trial and epidemiology of diabetes interventions and complications participants with type 1 diabetes. *Diabetes* **54,** 3103–3111
47. Meerwaldt, R., Hartog, J. W., Graaff, R., Huisman, R. J., Links, T. P., den Hollander, N. C., Thorpe, S. R., Baynes, J. W., Navis, G., Gans, R. O., and Smit, A. J. (2005) Skin autofluorescence, a measure of cumulative metabolic stress and advanced glycation end products, predicts mortality in hemodialysis patients. *J. Am. Soc. Nephrol.* **16,** 3687–3693
48. Cerami, C. F. H., Nicholl, I., Mitsuhashi, T., Giordano, D., Vanpatten, S., Lee, A., Al-Abed, Y., Vlassara, H., Bucala, R., and Cerami A, (1997) Tobacco smoke is a source of toxic reactive glycation products. *Proc. Natl. Acad. Sci. U. S. A.* **94,** 15–20
49. Scott, W. K., Schmidt, S., Hauser, M. A., Gallins, P., Schnetz-Boutaud, N., Spencer, K. L., Gilbert, J. R., Agarwal, A., Postel, E. A., Haines, J. L., and Pericak-Vance, M. A. (2007) Independent effects of complement factor H Y402H polymorphism and cigarette smoking on risk of age-related macular degeneration. *Ophthalmology* In press
50. Duan, Y., Mo, J., Klein, R., Scott, I. U., Lin, H. M., Caulfield, J., Patel, M., and Liao, D. (2006) Age-related macular degeneration is associated with incident myocardial infarction among elderly Americans. *Ophthalmology* **114,** 732–737
51. Thomas, M. C., Tsalamandris, C., MacIsaac, R., Medley, T., Kingwell, B., Cooper, M. E., and Jerums, G. (2004) Low-molecular-weight AGEs are associated with GFR and anemia in patients with type 2 diabetes. *Kidney Int.* **66,** 1167–1172

Received for publication March 1, 2007.
Accepted for publication May 10, 2007.